

Autonomous Underwater Vehicles: Development and Implementation of Time and Energy Efficient Trajectories¹

Monique Chyba, Thomas Haberkorn, Ryan N. Smith, Song K. Choi, University of Hawaii²

1 Introduction

Autonomous underwater vehicles (AUVs) are increasingly used, both in military and civilian applications. These vehicles are limited mainly by the intelligence we give them and the life of their batteries. Research is active to extend vehicle autonomy in both aspects. Our intent is to give the vehicle the ability to adapt its behavior under different mission scenarios (emergency maneuvers versus long duration monitoring). This involves a search for optimal trajectories minimizing time, energy or a combination of both.

Despite some success stories in AUV control, optimal control is still a very underdeveloped area. Adaptive control research has contributed to cost minimization problems, but vehicle design has been the driving force for advancement in optimal control research. We look to advance the development of optimal control theory by expanding the motions along which AUVs travel. Traditionally, AUVs have taken the role of performing the long data gathering mission in the open ocean with little to no interaction with their surroundings, *MacIver et al. (2004)*. The AUV is used to find the shipwreck, and the remotely operated vehicle (ROV) handles the exploration up close. AUV mission profiles of this sort are best suited through the use of a torpedo shaped AUV, *Bertram and Alvarez (2006)*, since straight lines and minimal (0° - 30°) angular displacements are all that are necessary to perform the transects and grid lines for these applications. However, the torpedo shape AUV lacks the ability to perform low-speed maneuvers in cluttered environments, such as autonomous exploration close to the seabed and around obstacles, *MacIver et al. (2004)*. Thus, we consider an agile vehicle capable of movement in six degrees of freedom without any preference of direction.

2 Model

The test-bed AUV which we use for our experiments is the Omni-Directional Intelligent Navigator (ODIN). ODIN is owned and operated by the Autonomous Systems Laboratory (ASL), College of Engineering at the University of Hawaii (UH). The experiments are carried out at the Duke Kahanamoku Swimming Complex at UH. ODIN has a spherical hull which is 65 cm in diameter. This sphere is constructed from an aluminum alloy to prevent corrosion. Eight thrusters are attached to the sphere via four fabricated mounts, each holding two thrusters. The thrusters are evenly distributed around the sphere with four vertical and four horizontal. ODIN is capable of moving in 6 degrees-of-freedom (DOF) from either a remote or autonomous mode. For our experiments, ODIN is tethered, but only to send commands via TCP/IP protocol from a shore based laptop to be run in an autonomous mode. This setup allows for multiple tests to be conducted without removing ODIN from the water to upload mission sorties. ODIN's internal CPU is a 800 MHz Intel based processor running on a PC104+ form factor with two external I/O boards providing A/D and D/A operations. Major internal components include a pressure sensor, internal navigation sensor and 24 batteries. ODIN is capable to compute real time, yaw, pitch, tilt, and depth and can run autonomously for up to 5 hours. However the yaw sensor is not designed to follow fast changes of heading ($\geq 6^\circ/s$). ODIN does not currently have real time sensors to detect horizontal (x, y) position. Instead, experiments are video taped from the 10m diving platform, giving us a near nadir view of ODIN's movements. Videos are saved and horizontal position is post processed for later analysis. A real time system utilizing sonar was available on ODIN, but was abandoned for two main reasons. First, the sonar created too much noise in the diving well

¹Research supported by NSF grant DMS-030641 and DMS-0608583 and partially supported by ONR grant #N00014-03-1-0969, #N00014-04-1-0751 and #N00014-04-1-0751.

²University of Hawaii - MATH, ORED, ASL, 2565 McCarthy Mall, Honolulu, Hawaii 96822, USA, mchyba@math.hawaii.edu

and led to inaccuracies. More significantly, in the implementation of our optimal trajectories, ODIN is often required to achieve large ($> 15^\circ$) list angles which render the sonars useless for horizontal position. Many solutions were attempted and video led to the most accurate results.

The equations of motion for a submerged rigid body have been extensively studied, *Fossen (1996)*. We will not repeat the derivation of these equations and refer the interested reader to *Chyba et al. (2007a)*, *Leonard (1996,1997)* for a more mathematical treatment. We here restrict ourselves to state these equations under the following assumptions. We assume that the body is immersed in a real fluid and that the origin of the body-fixed frame is the center of gravity $\vec{x}_g = \{x_g, y_g, z_g\}$. Moreover, based on our test-bed vehicle, we assume to have three planes of symmetry with body axes which coincide with the principal axes of inertia.

We denote the position and the orientation of our AUV respectively by the vector b and the rotation matrix R . The translational and angular velocities in the body-fixed frame are denoted by $\nu = (u, v, w)^t$ and $\Omega = (p, q, r)^t$, respectively, Fig.1. Our assumptions on the vehicle imply that the body inertia, the added mass and the moment of inertia matrices are diagonal, and the added mass cross-terms are zero. It follows that the total kinetic energy of our rigid body submerged in an unbounded real fluid is given by $T = \frac{1}{2}(\nu^t(mI_3 + M_f)\nu + \Omega^t(J_b + J_f)\Omega)$ where m is the mass of the vehicle, I_3 is the 3×3 -identity matrix and J_b is the vehicle inertia matrix. Moreover, M_f, J_f are respectively referred to as the added mass and the added moments of inertia which are assumed to be constant. In the sequel we will use $M = mI_3 + M_f$ and $J = J_b + J_f$.

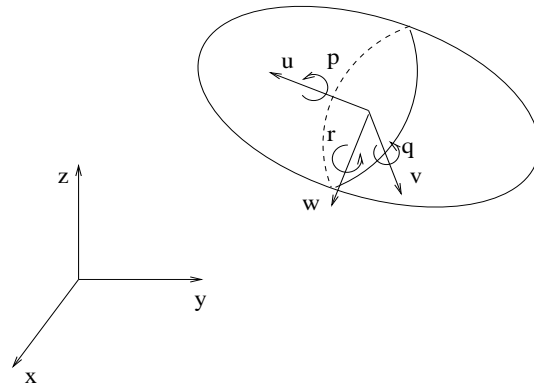


Fig.1: Earth-fixed and body-fixed frame

Gravity, buoyancy, drag and lift can be modeled using external forces and torques. The equations of a rigid body submerged in water are:

$$M\dot{\nu} = M\nu \times \Omega + D_\nu(\nu)\nu + R^t \rho g \mathcal{V} k + \varphi_\nu \quad (1)$$

$$J\dot{\Omega} = J\Omega \times \Omega + M\nu \times \nu + D_\Omega(\Omega)\Omega - r_B \times R^t \rho g \mathcal{V} k + \tau_\Omega \quad (2)$$

where the matrices $D_\nu(\nu), D_\Omega(\Omega)$ represent the drag force and momentum respectively. We also have a restoring force and a restoring moment. The only moment due to the restoring forces is the torque from the buoyancy force $-r_B \times R^t \rho g \mathcal{V} k$ where r_B is the vector from \vec{x}_g to the center of buoyancy $\vec{x}_B = \{x_B, y_B, z_B\}$. ρ is the fluid density, g the acceleration of gravity, \mathcal{V} the volume of fluid displaced by the rigid body and k the unit vector pointing in the direction of gravity. The forces $\varphi_\nu = (\varphi_u, \varphi_v, \varphi_w)^t$ and $\tau_\Omega = (\tau_p, \tau_q, \tau_r)^t$ account for the control.

For our computations and experiments we make the following assumptions. We assume a drag force $D_\nu(\nu)$ and a drag momentum $D_\Omega(\Omega)$, neglecting the off-diagonal terms. Based on our test-bed vehicle, our computations for the total drag forces for various velocities are approximated well using a cubic function with no quadratic or constant term. To summarize, the contribution to the translational motions is given by $D_\nu(\nu) = \text{diag}(D_\nu^{i1}\nu_i^3 + D_\nu^{i2}\nu_i)$ and to the rotational motions by $D_\Omega(\Omega) = \text{diag}(D_\Omega^{i1}\Omega_i^3 + D_\Omega^{i2}\Omega_i)$ where $D_\nu^{ij}, D_\Omega^{ij}$ are constant coefficients.

In local coordinates, the equations of motion for a submerged rigid body in a real fluid are as follows. We denote by $\eta = (x, y, z, \phi, \theta, \psi)^t$ the position and orientation of the vehicle with respect to the earth-fixed reference frame. The coordinates ϕ, θ, ψ are the Euler angles for the body frame. The coordinates corresponding to translational and rotational velocities in the body frame are $\nu = (u, v, w)^t$ and $\Omega = (p, q, r)^t$. We have:

$$\dot{x} = u \cos \psi \cos \theta + v R^{12} + w R^{13} \quad (3)$$

$$\dot{y} = u \sin \psi \cos \theta + v R^{22} + w R^{23} \quad (4)$$

$$\dot{z} = -u \sin \theta + v \cos \theta \sin \phi + w \cos \theta \cos \phi \quad (5)$$

$$\dot{\phi} = p + q \sin \phi \tan \theta + r \cos \phi \tan \theta \quad (6)$$

$$\dot{\theta} = q \cos \phi - r \sin \phi \quad (7)$$

$$\dot{\psi} = \frac{\sin \phi}{\cos \theta} q + \frac{\cos \phi}{\cos \theta} r \quad (8)$$

$$\dot{u} = \frac{1}{m_1} [-(m_3)wq + (m_2)vr + D_\nu(u) - G \sin \theta + \varphi_u] \quad (9)$$

$$\dot{v} = \frac{1}{m_2} [(m_3)wp - (m_1)ur + D_\nu(v) + G \cos \theta \sin \phi + \varphi_v] \quad (10)$$

$$\dot{w} = \frac{1}{m_3} [-(m_2)vp + (m_1)uq + D_\nu(w) + G \cos \theta \cos \phi + \varphi_w] \quad (11)$$

$$\begin{aligned} \dot{p} = & \frac{1}{I_x + J_f^p} [(I_y - I_z + J_f^q - J_f^r)qr + (M_f^v - M_f^w)vw \\ & + D_\Omega(p) + \rho g \mathcal{V}(-y_B \cos \theta \cos \phi + z_B \cos \theta \sin \phi) + \tau_p] \end{aligned} \quad (12)$$

$$\begin{aligned} \dot{q} = & \frac{1}{I_y + J_f^q} [(I_z - I_x + J_f^r - J_f^p)pr + (M_f^w - M_f^u)uw \\ & + D_\Omega(q) + \rho g \mathcal{V}(z_B \sin \theta + x_B \cos \theta \cos \phi) + \tau_q] \end{aligned} \quad (13)$$

$$\begin{aligned} \dot{r} = & \frac{1}{I_z + J_f^r} [(I_x - I_y + J_f^p - J_f^q)pq + (M_f^u - M_f^v)uv \\ & + D_\Omega(r) + \rho g \mathcal{V}(-x_B \cos \theta \sin \phi - y_B \sin \theta) + \tau_r] \end{aligned} \quad (14)$$

where $G = mg - \rho g \mathcal{V}$, $m_i = m + M_f^{\nu_i}$, $D_\nu(\nu_i) = D_\nu^{i1} \nu_i^3 + D_\nu^{i2} \nu_i$ and $D_\Omega(\Omega_i) = D_\Omega^{i1} \Omega_i^3 + D_\Omega^{i2} \Omega_i$. $\varphi_\nu = (\varphi_u, \varphi_v, \varphi_w)$ and $\tau_\Omega = (\tau_p, \tau_q, \tau_r)$ represent the control.

The numerical values of the various parameters used for the model are given in Table I. These values were derived from experiments performed on ODIN. The added mass and drag terms were estimated from formulas found in *Allmendinger (1990)* and *Imlay (1961)*. Moments of inertia were calculated using experiments outlined in *Bhattacharyya (1978)*. We used inclining experiments to determine \vec{x}_B . Hydrodynamic parameters are verified and refined through model testing at a one-to-one scale.

Table I: Numerical values for hydrodynamic coefficients

m	126.55 kg	$\rho g \mathcal{V}$	1243.19 N	\vec{x}_B	(0.49, 0.34, -7) mm
M_f^u	70 kg	M_f^v	70 kg	M_f^w	70 kg
I_x	5.46 kgm ²	I_y	5.29 kgm ²	I_z	5.72 kgm ²
J_f^p	0 kgm ²	J_f^q	0 kgm ²	J_f^r	0 kgm ²
D_ν^{11}	-27.0273	D_ν^{21}	-27.0273	D_ν^{31}	-27.0273
D_ν^{12}	-897.6553	D_ν^{22}	-897.6553	D_ν^{32}	-897.6553
D_Ω^{11}	-13.793	D_Ω^{21}	-13.793	D_Ω^{31}	-11.9424
D_Ω^{12}	-6.4594	D_Ω^{22}	-6.4594	D_Ω^{32}	-6.9393

Unique to ODIN's construction is the control from an eight-dimensional thrust to move in six DOF. This construction puts redundancy into the system in case of thruster failure. ODIN is able to operate in an under-actuated condition if necessary, and research is active in this area. It is important

to distinguish between the control for the real vehicle, namely the applied control referring to the action of the eight thrusters, and the six DOF in the equations of motion (4). Our input trajectories to ODIN take the form of the six DOF controls which are converted on-board ODIN to the eight-dimensional actual thrusters using the following Thrust Control Matrices (TCM's):

$$\text{TCM}_{\text{horizontal}} = \begin{pmatrix} -0.707 & 0.707 & 0.707 & -0.707 \\ 0.707 & 0.707 & -0.707 & -0.707 \\ 0.48160 & -0.48160 & 0.48160 & -0.48160 \end{pmatrix} \quad (15)$$

$$\text{TCM}_{\text{vertical}} = \begin{pmatrix} -1.0 & -1.0 & -1.0 & -1.0 \\ -0.26989 & -0.26989 & 0.26989 & 0.26989 \\ 0.26989 & -0.26989 & -0.26989 & 0.26989 \end{pmatrix} \quad (16)$$

More details on the derivation of these matrices can be found in *Chyba et al. (2007b)*. In the sequel, we assume the control domain for the force components φ_ν and τ_Ω to be limited by upper and lower limits that we denote by $\alpha_{\nu_i}^{\min}, \alpha_{\Omega_i}^{\max}$. A control is said to be admissible if it takes its value within these bounds. For our numerical computations, we will take $\alpha_{u,v}^{\max} = -\alpha_{u,v}^{\min} = 8$ N, $\alpha_w^{\max} = 30$ N, $\alpha_w^{\min} = -5$ N, $\alpha_{p,q}^{\max} = -\alpha_{p,q}^{\min} = 3$ Nm and $\alpha_r^{\max} = -\alpha_r^{\min} = 1$ Nm. The non symmetry of $\alpha_w^{\min,\max}$ is due to the fact that the 4 vertical thrusters are all oriented in the same direction which is shown by the 4 negative coefficients in the first row of the matrix (16). Along with the tests to determine the values in Table I, we also tested the thrusters. Each thruster has a unique voltage input to power output relationship. This relationship is highly nonlinear and is approximated using a piecewise linear function which we refer to as our thruster model.

3 Maximum Principle

The maximum principle as developed in the 1950's, *Pontryagin et al. (1962)*. This principle provides necessary conditions for a trajectory to be optimal with respect to a given cost. *Chyba et al. (2007a)* present a theoretical analysis based on the maximum principle. Our goal here is to introduce the terminology to describe the trajectories that we will consider for our motion planning problem, namely the notion of bang-bang and singular arcs.

We introduce $\chi = (\eta, \nu, \Omega)$, and let $\chi_0 = \chi(0)$ and $\chi_T = \chi(T)$ be the initial and final states for our vehicle. We denote the control $\varphi = (\varphi_\nu, \tau_\Omega)$. Then, the equations of motion can be written as an affine control system:

$$\dot{\chi}(t) = Y_0(\chi(t)) + \sum_{i=1}^6 Y_i(t)\varphi_i(t) \quad (17)$$

where the drift Y_0 accounts for the centripetal, Coriolis, drag and restoring forces. The input vector fields are given by $Y_i = (0, 0, I_i^{-1})^t$ with I_i^{-1} being the column i of the matrix $I^{-1} = \begin{pmatrix} M^{-1} & 0 \\ 0 & J^{-1} \end{pmatrix}$.

Let us now assume that we want to minimize a cost determined by the following expression: $C = \int_{t_0}^{t_1} f^0(\chi(t), \varphi(t)) dt$. This cost can represent the time ($f^0 = 1$), energy consumption (to be discussed later in this paper) or a combination of both.

An admissible cost-optimal control $\varphi = (\varphi_\nu, \tau_\Omega)$ defined on $[0, T]$ with corresponding trajectory $\chi = (\eta, \nu, \Omega)$ solution of (17) steering the body from χ_0 to χ_T satisfies

$$\dot{\eta} = \frac{\partial H}{\partial \lambda_\eta}, \dot{\nu} = \frac{\partial H}{\partial \lambda_\nu}, \dot{\Omega} = \frac{\partial H}{\partial \lambda_\Omega}, \quad \dot{\lambda}_\eta = -\frac{\partial H}{\partial \eta}, \dot{\lambda}_\nu = -\frac{\partial H}{\partial \nu}, \dot{\lambda}_\Omega = -\frac{\partial H}{\partial \Omega} \quad (18)$$

where $\lambda = (\lambda_\eta, \lambda_\nu, \lambda_\Omega)$ is a twelf-component vector. $(\lambda_0, \lambda(t)) \neq 0$ for all t . The function H is given by:

$$H(\chi, \lambda, \varphi, \tau) = \lambda_\eta^t (R\nu, \Theta\Omega)^t + \lambda_\nu^t M^{-1} [M\nu \times \Omega + D_\nu(\nu)\nu + R^t \rho g \mathcal{V}k + \varphi_\nu] + \lambda_\Omega^t J^{-1} [J\Omega \times \Omega + M\nu \times \nu + D_\Omega(\Omega)\Omega - r_B \times R^t \rho g \mathcal{V}k + \tau_\Omega] + \lambda_0 f^0(\chi, \varphi) \quad (19)$$

Furthermore, the maximum condition holds: $H(\chi(t), \lambda(t), \varphi_\nu(t), \tau_\Omega(t)) = \max_\gamma H(\chi(t), \lambda(t), \gamma_1, \gamma_2)$. The maximum of the Hamiltonian is constant along the solutions of (18). A quadruple $(\chi, \lambda, \varphi_\nu, \tau_\Omega)$ that satisfies the maximum principle is called an extremal, and the vector function $\lambda(\cdot)$ is called the adjoint vector.

4 Minimum Time

4.1 Singular and bang-bang arcs

In this case we have $f^0(\chi, \varphi) = 1$. The maximum condition, along with the control domain, intuitively expresses the fact that to be time optimal the thrusters must operate at their extreme values for the duration of the trajectory. However, to maintain a prescribed orientation the vehicle must also apply small thrusts for any minor corrections that are needed. These concepts will be clearly shown in the examples provided in the next section. The above control strategies are known as bang-bang (saturation of the thrust on a given interval) and singular (low thrust application on an interval for small corrections). More formally, we can summarize the previous comments as follows. Condition is equivalent almost everywhere to $(M, J$ diagonal and positive), $i = 1, 2, 3$:

$$\varphi_{\nu_i}(t) = \begin{cases} \alpha_{\nu_i}^{\min} & \text{for } \lambda_{\nu_i}(t) < 0 \\ \alpha_{\nu_i}^{\max} & \text{for } \lambda_{\nu_i}(t) > 0 \end{cases} \quad (20)$$

$$\tau_{\Omega_i}(t) = \begin{cases} \alpha_{\Omega_i}^{\min} & \text{for } \lambda_{\Omega_i}(t) < 0 \\ \alpha_{\Omega_i}^{\max} & \text{for } \lambda_{\Omega_i}(t) > 0 \end{cases} \quad (21)$$

The isolated zeros of the switching functions λ_{ν_i} , λ_{Ω_i} correspond to the switching of the thrusters between their two extreme values. A bang-bang control only takes values of α_i^{\min} or α_i^{\max} . On the other hand, if there is a nontrivial interval $[t_1, t_2]$ such that a switching function is identically zero, the corresponding control is said to be singular on that interval.

As a final remark, we would like to point out that indirect methods are numerical methods based on the Maximum Principle. The strategy is to rewrite the optimal control problem into a two-point boundary value problem with the differential system being the Hamiltonian. These methods, called shooting methods, are very accurate when they converge, however in our case it would be very hard to achieve the convergence due to the bang-singular structure of the time optimal strategies in the case of the AUV's. This is why we base our strategy on direct methods as explained in the next section.

4.2 Numerical computation

A direct method is used for our numerical computations. It is based on the rewriting of the optimal control problem (OCP) into a finite dimensional nonlinear optimization problem (NLOP). The variables of the NLOP are the discretized state and control of the OCP. The constraints of this NLOP are the dynamic constraints; the upper and lower bounds on the control and the final state constraint. Methods to solve nonlinear optimization problems are well developed and we choose to use the interior point IpOpt, *Wächter and Biegler (2006)*, in conjunction with the modeling Language AMPL, *Fourer et al. (1993)*.

Due to our experimental setting we choose the initial configuration η_0 to be the origin and the final configuration $\eta_f = (5, 4, 1, 0, 0, 0)$, both at zero velocity. The limitation on the size of the trajectory is bounded by the size of the field of vision of the camera shooting the experiments (~ 5 m by 7 m).

There exists a trajectory between every pair of configurations at rest. Indeed, by only considering pure motions along or about one body fixed-frame axis at the time, we can realize such a trajectory with at most 6 pure motions. For our pair of configurations we need a pure surge, a pure sway and a pure heave. If we saturate the corresponding translational controls the total duration of the trajectory is $t_{pure} \approx 72.77$ s.

Numerically solving the minimum time problem for our pair of configurations provides a trajectory with a final time $t_{NLOP}^f \approx 23.47$ s. It is less than half the time for the pure motion strategy. Fig.2 shows the minimum time control strategy and trajectory.

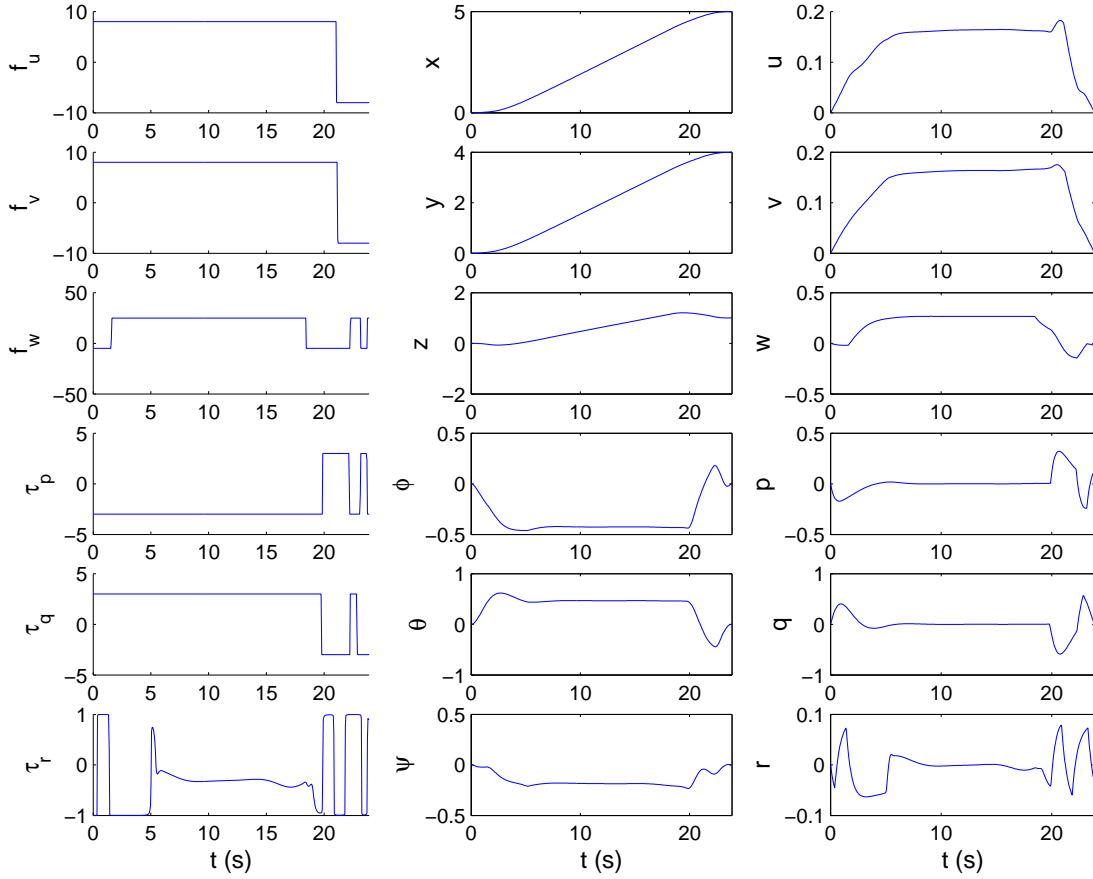


Fig.2: Minimum-time trajectory, $\eta_f = (5, 4, 1, 0, 0, 0)$

The minimum time strategy displays a large number of switchings. We also have a singular arc for the τ_r control (yaw component). This singular arc emphasizes the need for the AUV to maintain a prescribed orientation in order to maximize translational controls. Such a trajectory is attractive because it is time optimal, however its implementation on a real vehicle is impossible. Indeed, close switching times are potentially damaging to the thrusters, and in fact, thrusters are physically unable to adjust to rapid switches. An additional concern is the singular arc. A control strategy that is continuously changing requires a great amount of data to be stored in the AUV's memory. Numerically, NLOP is time consuming since we need a fine discretization due to the singular arcs. Since the finer the discretization, the larger the problem, we rapidly encounter problems with tens of thousands of variables (12 states and 6 controls per discretization step).

Practical considerations show the need for a trajectory to be both time efficient and implementable. A compromise between pure motions trajectories and time optimal trajectories is our goal.

First we consider a translational displacement. We can realize trajectory designs which are time efficient and implementable by considering motions with piecewise constant controls containing only one common switching time. If there are no angular velocities, then the evolutions of u , v and w are completely decoupled. Then, given two configurations, a switching time and final time, one can always find six values of control (two values per translational control) that realize the translational motion. These values of control might be out of the bounds of the thrusters. This is solved by increasing the switching time and the final time. This is also true if there are initial or/and final translational velocities, provided they are reachable with the allocated control bounds.

Next, we extend this construction to all dimensions of the configuration space (namely the orientations), except we may be required to use more than one common switching time. Applying this idea we can choose to discretize our OCP, but only with a restricted number of discretization points;

typically not more than 10, versus the 1000 plus for NLOP. The difference between this rewriting and the previous is that we take the values of the constant control and the switching times as the unknowns of the optimization problem. The new optimization problem, called the Switching Time Parameterization Problem STPP_p takes the following form:

$$\text{STPP}_p \begin{cases} \min_{z \in \mathcal{D}} t_{p+1} \\ t_0 = 0 \\ t_{i+1} = t_i + \xi_i, \quad i = 1, \dots, p \\ \chi_{i+1} = \chi_i + \int_{t_i}^{t_{i+1}} \dot{\chi}(t, \varphi_i, \tau_i) dt \\ \chi_{p+1} = \chi_f \\ z = (\xi_1, \dots, \xi_{p+1}, \varphi_1, \tau_1, \dots, \varphi_{p+1}, \tau_{p+1}) \\ \mathcal{D} = \mathbb{R}_+^{(p+1)} \times \mathcal{U}^{(p+1)} \end{cases} \quad (22)$$

An interesting feature of STPP is that with the low number of switching times p , it is possible to use a high-order integrator to compute the dynamic constraint. This leads to a very accurate solution with respect to the theoretical model. For practical purposes we also smooth the switchings with linear functions so they do not occur instantaneously.

Applying the nonlinear solver IpOpt to STPP_p, we get final times that are close to the computed minimum time, as shown in Table I. The first column corresponds to a given final configuration (at rest), the second to the minimum time, the third to the pure motion time, the third, fourth and fifth to STPP_p times with 1, 2 and 5 switchings, respectively. The STPP_p solutions all contain linear junctions, 120 ms wide, between 2 constant thrust arcs. For all these motions we take the initial configuration to be the origin.

Table I: Minimum time, pure motion time and selected STPP_p times

η_f	t_{NLOP}^f (s)	t_{pure}^f (s)	$t_{STPP_1}^f$ (s)	$t_{STPP_2}^f$ (s)	$t_{STPP_5}^f$ (s)
(5, 4, 1, 0, 0, 0)	23.47	72.77	35.90	25.29	23.93
(5, 3, 0, 0, 0, 0)	23.04	59.18	35.90	28.89	24.46
(5, 0, 0, 0, 0, 0)	21.36	35.84	35.90	26.83	22.60
(2, 1, 0, 0.2, 0.2, 0)	11.77	30.75	16.40	14.46	12.94
(3, 4, 0, 0, 0.2, 1)	20.93	66.91	31.86	24.64	21.87

The final times of the STPP_p method are close to the minimum time even for $p = 1$, especially if we take the pure motion time as a comparison. We should note that if NLOP and STPP_p have the same number of discretization steps, then STPP_p yields a shorter time because its set of admissible control strategies contain the set of NLOP (by the variable ξ_i). Thus we have the following inequalities:

$$t_{\min}^f \leq t_{STPP_{p+1}}^f \leq t_{STPP_p}^f \leq t_{NLOP_p}^f \quad (23)$$

The first three entries for STPP₁ are the same. This is not surprising since STPP₁ will give the smallest switching and final times for which the straight line control strategy (without change of orientation) is feasible while keeping the controls within the bounds of the thrusters. And, those times are limited here by the largest of the surge, sway and heave displacements.

Another advantage of STPP is that it is computationally efficient since the number of variables of STPP_p is $7(p + 1)$; this is less than 50 for $p = 5$. In the cases in which it converges, STPP_p is computationally much faster than NLOP.

Fig.3 shows the trajectory for STPP₂ with final position $\eta_f = (5, 4, 1, 0, 0, 0)$. Here the control strategy is easier to implement on a real vehicle than the time minimum strategy shown in Fig.2. The difference between the time optimal strategy and the STPP one is the fewer changes in the orientation along the STPP strategy. This is directly due to the low number of switchings. The surge

and sway control contain one switching time and the important gain of time realized when adding a second switching time is due to the possibility of changing the orientation during the transfer, which is impossible when only one switching time is allowed.

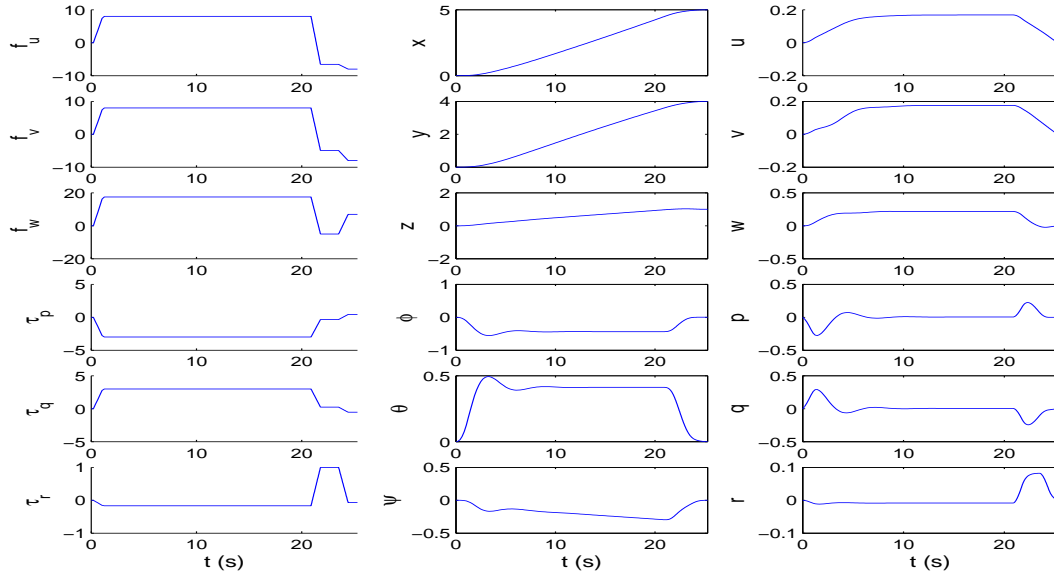


Fig.3: STPP₂ trajectory for $\eta_f = (5, 4, 1, 0, 0, 0)$

For ODIN, a change of control implies a control change for at least 4 thrusters, which means a single switching strategy is easier to implement than the pure motion strategy. This is only true when considering the number of switchings of the actual thrusters, but false if we consider that a pure motion implementation can be complemented with a feedback stabilization.

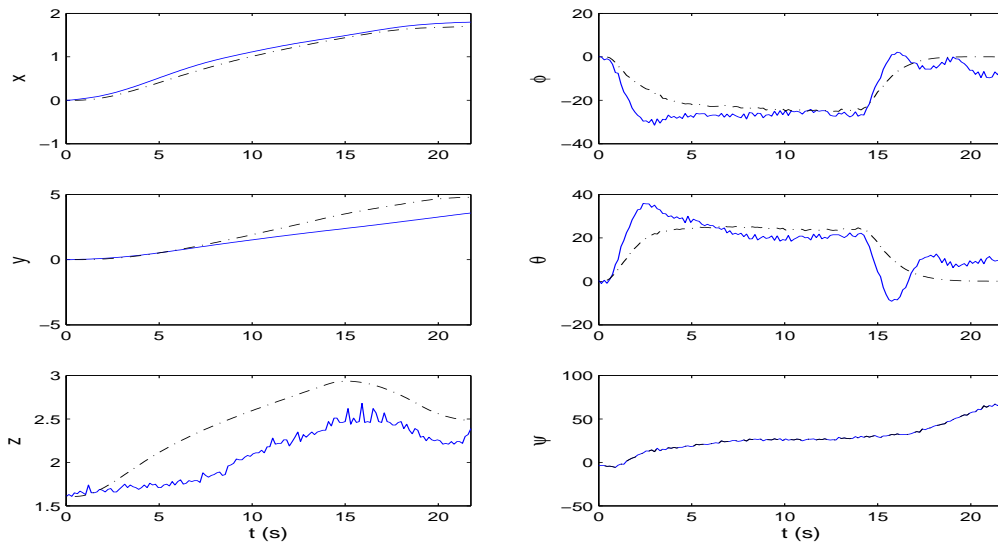


Fig.4: STPP₂ experimental (plain) and theoretical (dashed) trajectories for $\eta_f = (5, 4, 1, 0, 0, 0)$

If we consider the STPP method for the eight-dimensional actual thrusters control rather than the six DOF controls, we are still able to compute time-efficient trajectories. Fig.5 shows a STPP₂ control strategy on the control domain Υ . The minimum time for this case is $t_{STPP_2, \Upsilon}^f \approx 19.69$ s. This is faster than the time computed for the NLOP. This is due to the transformation of the real control domain through the Thruster Control Matrix (15)-(16). This transformation forces a restriction of the

six DOF control domain to a smaller control domain than allowed by the eight dimensional control. In order to compare this with Fig.3, we also display the control strategy given by (φ, τ) . The STPP₂ trajectory is faster since the bounds on the thrusters are loosened, thus, the switchings are of greater magnitude. There is no yaw control τ_r applied along this trajectory since all the horizontal thrust is used for φ_u and φ_v . Despite the implementability of this trajectory, the unique and unbalanced thruster behavior in conjunction with the larger magnitude thrusts exaggerates errors here more than in the six-dimensional STPP strategy. Thus, we restrict ourselves to the initial six DOF control domain to minimize the effect of the thrusters' dynamic differences, over which we have no control.

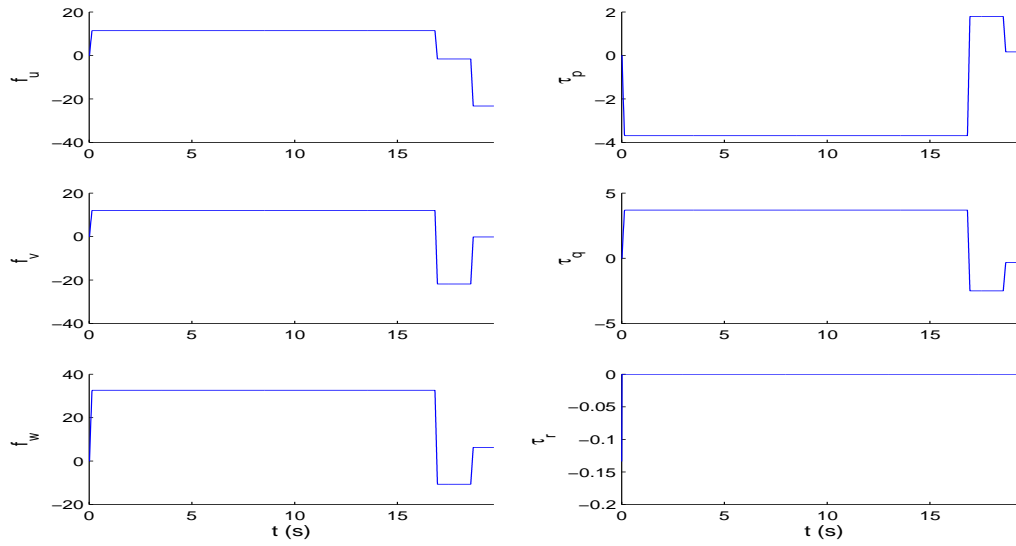


Fig.5: STPP₂ trajectory for $\eta_f = (5, 4, 1, 0, 0, 0)$ and control domain Υ

4.3 Experiments

Fig.6 shows the result of the implementation of a pure motion trajectory onto ODIN. The pure motion open-loop control in surge, sway and heave is complemented with a feedback control on pitch, roll and yaw. This feedback on orientation compensates for the physical unbalancing of the thrusters. We represent the surge and sway evolution in the picture. The solid line is the actual trajectory realized by ODIN. The dotted line represents the trajectory obtained using our theoretical model with the thrusts actually applied to ODIN during the test. In the theoretical model, we impose the yaw evolution to be that of experiment, otherwise the horizontal direction diverges very fast due to the sensitivity of the yaw (no restoring moment in yaw).

Fig.6 validates our theoretical model. Despite many challenges in experimentation at the pool, we observed excellent behavior by ODIN. The difference in heading is the result of our inertial measurement unit's sensitivity to the surrounding magnetic field generated by pool's metal wall and the recirculation pumps. The small difference in surge and sway magnitude are due to factors such as underestimation of damping, imperfection in thruster modeling, pool current and the drag induced by the umbilical tether. The drag from the tether greatly depends on the tether location at the beginning of an experiment. This drag is difficult to take into account due to its variance. The current in the pool is dependent on location and is currently under investigation.

Fig.4 shows the experimental evolution of the implementation of the STPP₂ control strategy of Fig.3. For comparison, we display the theoretical behavior of the AUV for which the yaw evolution has been corrected similarly to the pure motion analysis. In this experiment, we do not use any feedback control. We obtained a very good response from ODIN. Its trajectory closely follows the theoretical one. However, the heave evolution is not reliable which comes from the drag and slight positive buoyancy of the tether. ODIN is only positively buoyant by only 3 N, thus any change

in buoyancy will have a noticeable impact on the depth evolution. The surge and sway are also influenced by the drag of the tether and pool current which explains the theoretical over estimation of their evolutions. We see an overshooting in the pitch and roll experimental evolution. This is partially due to the un-modeled transient behavior of the thrusters.

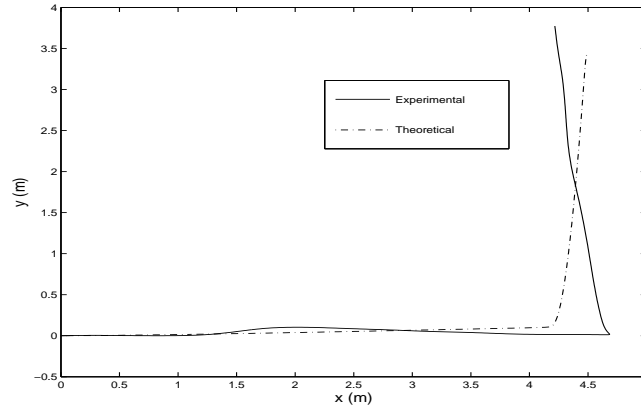


Fig.6: Pure motion experimental surge, sway evolution and the theoretical evolution (with yaw correction) $\eta_f = (5, 4, 1, 0, 0, 0)$

5 Minimum Energy Consumption

5.1 Criterion

Since we are able to design practical time-efficient trajectories, we now consider an energy criterion. Such a criterion is directly related to the physical model considered. Since AUV's are powered by internal batteries, we consider maximization of the life span of the batteries. The majority of the energy consumption of an AUV is the thrusters, while the on-board computer and sensors only play a marginal role. For ODIN, the thrusters are powered by a constant 24 V. We represent the consumption of one thruster by the current it pulls. Since the life span of a battery is given in Ampere-hour, the criterion to consider for one thruster is the integral of the pulled current over the trajectory duration. Since ODIN has eight thrusters, the criterion will have the form

$$J = \min \sum_{i=1}^8 \int_0^{t^f} I(\gamma_i(t)) dt \quad (24)$$

$\gamma_i(t)$ represents the thrust delivered by the i^{th} thruster and I is a function which gives the pulled current with respect to a given thrust. For simplicity, we assume I equal for all thrusters.

For the criterion J , we have three choices for the final time; we fix it, we introduce it into the criterion as a weighted final time to minimize, or we leave it free. Since our mechanical system is dissipative, the third choice will still yield a finite final time. Also, there exists a finite final time with minimum energy consumption such that any increase in time uses more energy to compensate the dissipative forces without gaining efficiency over the trajectory. Let us denote by t_{\min}^J the final time which yields the minimum consumption. Then any solution of the fixed final time minimum energy consumption with $t^f < t_{\min}^J$ will be a solution of the weighted minimum consumption and minimum time (the second choice) for a specific choice of weights.

We fix t^f as a multiple of the minimum time computed using the methods of Section 4: $t^f = c_{t^f} t_{\min}^f$ and $c_{t^f} > 1$. This problem does not have a solution for $c_{t^f} < 1$ and the solution for $c_{t^f} = 1$ is the minimum time solution.

Since criterion (24) explicitly involves the eight thrusters, the proper domain of controllability is the complete eight dimensional domain Υ . Indeed, if we insist on using the simplified six dimensional

control φ and τ we will encounter an intricate criterion. Hence, we use the eight dimensional control γ , remembering that φ and τ are obtained from γ through the linear transformations (15)-(16).

Computing the (OCP) associated to (24) depends on the function I . From experimental measurements, we conclude that an accurate approximation of I is a piecewise linear function:

$$I(\gamma) = \begin{cases} -0.192\gamma & = \alpha\gamma & \text{for } \gamma \leq 0 \\ 0.408\gamma & = \beta\gamma & \text{for } \gamma > 0 \end{cases} \quad (25)$$

C^2 -functions are usually required for a numerical optimizer to converge. Moreover, our criterion is non differentiable at the minimum of the pulled current. This is a critical point which plays an important role in minimization. Applying the maximum principle to J gives a control strategy of bang-bang controls connected by singular arcs. Thus, we first smooth J . For this, we consider two fourth-order polynomials P_α, P_β (covering the negative and positive γ respectively). These polynomials form a C^2 -junction P_α/P_β at zero, I/P_α at a negative thrust γ_α and P_β/I at a positive thrust γ_β . Let $\varepsilon > 0$ and $P_\alpha(0) = P_\beta(0) = \varepsilon$. This gives $P_\alpha(\gamma) = \alpha_4\gamma^4 + \alpha_3\gamma^3 + \varepsilon$ and $P_\beta(\gamma) = \beta_4\gamma^4 + \beta_3\gamma^3 + \varepsilon$ where α_i, β_i are uniquely defined. As ε tends to zero, I approaches the smoothed function. Let us call our smoothed current/force function I_ε and the corresponding smoothed criterion J_ε . See Fig.8 for a graphic illustration.

From the maximum principle, the structure of the eight-dimensional extremal control is given by eight functions κ_i , $i = 1, \dots, 8$. These functions are a linear combination of the adjoint variables $\lambda_{\nu_i, \Omega_i}$ with linear coefficients coming from the Thruster Control Matrix (15-16). See *Chyba et al. (2007b)* for more details.

5.2 Numerical results

We use the direct method NLOP to gain insight to such strategies. Multiple shooting methods are currently under investigation. Fully discretizing the OCP in state and control, we can again apply the IpOpt solver along with the modeling language AMPL. Despite the problem being significantly more sensitive, we can compute optimal solutions for a various collection of c_{tf} . For $\eta_f = (5, 4, 1, 0, 0, 0)$, we take $t_{\min}^f \approx 23.47$ s, the minimum time of the six-dimensional controlled system. Before looking at specific control strategies, we consider the evolution of energy consumption with respect to c_{tf} shown in Fig.7. In the right diagram of Fig.7, the criterion J is not minimized. So, it is not surprising to have an evolution depending on ε . As expected, J is not decreasing with c_{tf} , but has a minimum for some final time $t_{\min}^{J_\varepsilon}$ which depends on ε .

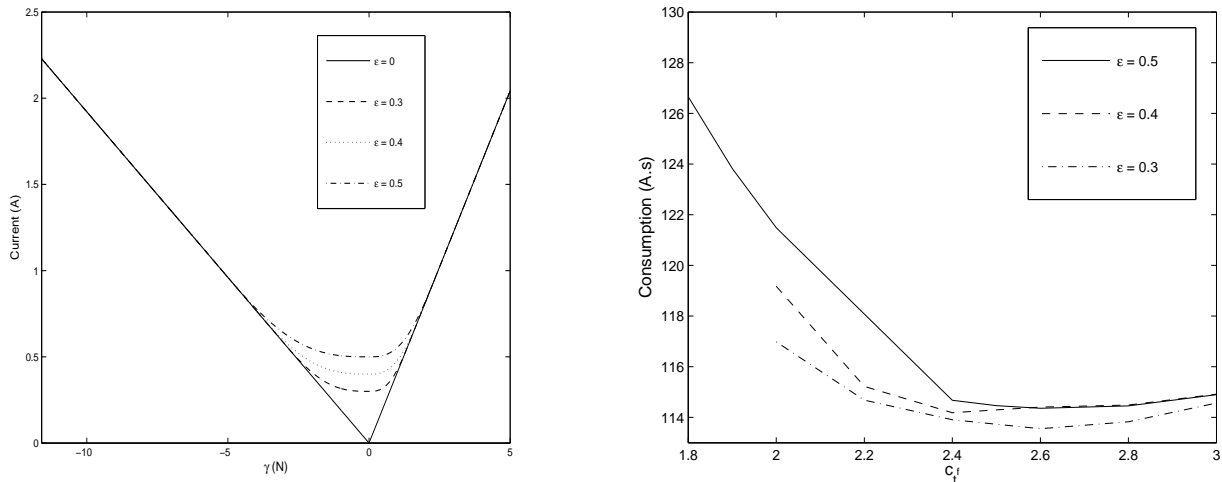


Fig.7: Smoothed function I_ε (left) and evolution of consumption J w.r.t. c_{tf} for $\eta_f = (5, 4, 1, 0, 0, 0)$ and $\varepsilon = 0.5, 0.4$ or 0.3 (right)

For initial configuration at the origin and $\eta_f = (5, 4, 1, 0, 0, 0)$, there are numerous minimum consumption strategies to consider. Nevertheless, a first choice is one that approximately corresponds to $t_{\min}^{J,\varepsilon}$. Fig.8 shows the thrust evolution and trajectory corresponding. We display the controls φ and τ rather than γ since they are more meaningful, even though they are not used in the optimization process. Compare this trajectory to the minimum-time trajectory in Fig.2. The first obvious difference is the magnitude of the control. For the minimum-consumption control strategy, there is minimal actuator saturation, while for the minimum-time strategy actuators are saturated for the entire motion.

The minimum-energy consumption strategies will be very hard to implement for two main reasons. First, the continuous evolution of the control strategy is not implementable on a real vehicle, and even a discretization would require the storage of impractical amounts of data. Secondly, considering low magnitude thrusts will exaggerate the ODIN's sensitivity to the unmodeled external forces such as a tether drag and pool current. For these reasons it would be interesting to adapt the STPP method to the energy consumption problem and consider final times which are closer to the minimum time. This will ensure a greater thrust magnitude while still saving energy.

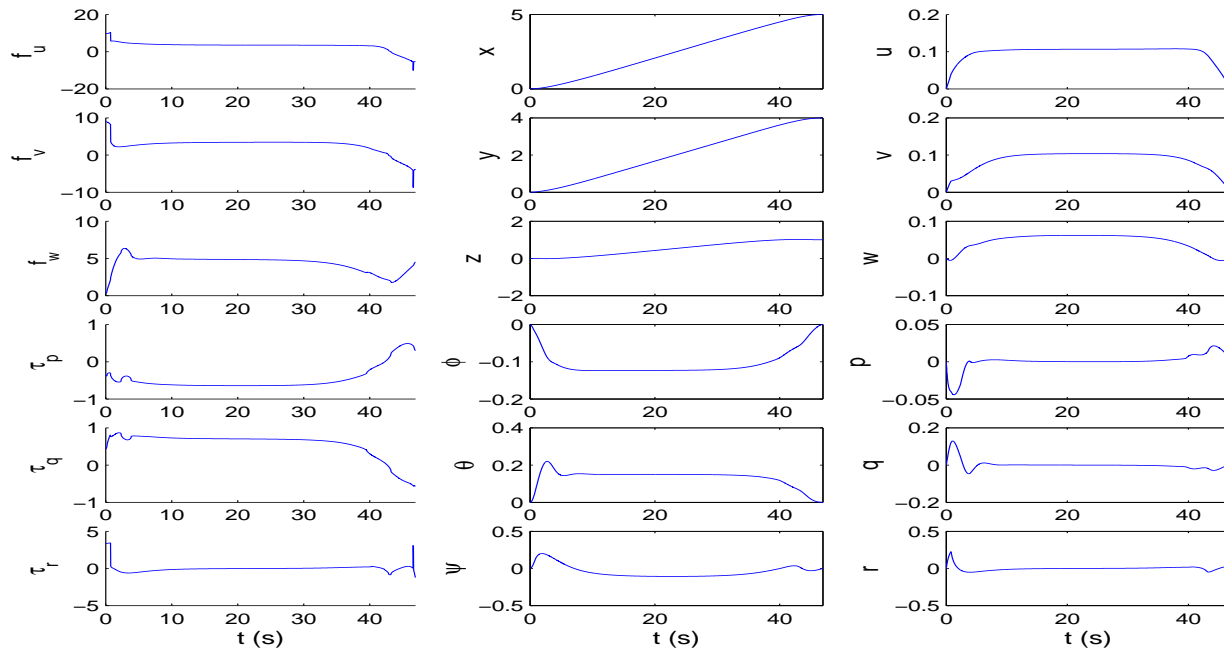


Fig.8: Minimum-consumption control strategy and trajectory for $\eta_f = (5, 4, 1, 0, 0, 0)$, $t^f = 46.93$ s and $\varepsilon = 0.5$

An adaptation of (STPP) should be feasible. Indeed, extremal strategies will contain constant thrust arcs of maximum and zero magnitude by the maximum principle applied to J . These strategies will be easier to implement than continuous evolutions provided we take precautions to smooth the transitions between thrust arcs.

References

- ALLMENDINGER, E. (1990), *Submersible vehicle design*, SNAME
- BERTRAM, V.; ALVAREZ, A. (2006), *Hydrodynamic aspects of AUV design*, 5th Conf. Computer and IT Applications in the Maritime Industries (COMPIT), Leiden, pp.45-53
- BHATTACHARYYA, R. (1978), *Dynamics of Marine Vehicles*, Wiley
- BULLO, F.; LEWIS, A.D. (2004), *Geometric Control of Mechanical Systems Modeling, Analysis, and Design*

for *Simple Mechanical Control Systems*, Springer-Verlag, New York-Heidelberg-Berlin, 49 in *Texts in Applied Mathematics*

CHYBA, M.; HABERKORN, T.; SMITH, R.N.; WILKENS, G.R. (2007a), *Geometric properties of singular extremals for a submerged rigid body*, Preprint University of Hawaii
<http://www.math.hawaii.edu/~mchyba/publications/index.htm>

CHYBA, M.; HABERKORN, T.; SMITH, R.N.; CHOI, S.K. (2007b), *Implementable efficient time and energy consumption trajectories design for an autonomous underwater vehicle*, 6th Conf. Computer and IT Applications in the Maritime Industries (COMPIT), Cortona, pp.443-457

FOSSEN, T.I. (1994), *Guidance and control of ocean vehicles*, Wiley, New York

FOURER, R.; GAY, D.M.; KERNIGHAN, B.W. (1993), *AMPL: A Modeling Language for Mathematical Programming*, Duxbury Press, Brooks-Cole Publ.

IMLAY, F.H. (1961), *The complete expressions for added mass of a rigid body moving in an ideal fluid*, Technical Report DTMB 1528

LEONARD, N.E. (1996), *Stabilization of steady motions of an underwater vehicle*, 35th IEEE Conf. Decision and Control

LEONARD, N.E. (1997), *Stability of a bottom-heavy underwater vehicle*, *Automatica* 33/3, pp.331-346

MacIVER, M.A.; FONTAINE, E.; BURDICK, J.W. (2004), *Designing future underwater vehicles: Principles and mechanisms of the weakly electric fish*, *IEEE J. Oceanic Eng.* 29/3

PONTRYAGIN, L.S.; BOLTYANSKI, B.; GAMKRELIDZE, R.; MICHTCHENKO, E.(1962), *The Mathematical Theory of Optimal Processes* Interscience, New York

WAECHTER, A.; BIEGLER, L.T. (2006), *On the implementation of an interior-point filter-line search algorithm for large-scale nonlinear programming*, Research Report RC 23149, IBM T.J. Watson Research Center, Yorktown

???? questions

there are still 'Hamiltonian' terms (two times)

Eq.(22) has an index $z \in \mathcal{D}$ and a \mathcal{D} that uses \times which is incomprehensible to me.